Deep-learning-enabled breathable thermogalvanic hydrogel array for self-powered mental monitoring

Yu Li,[a] Ning Li,[b] Xinru Zhang,[b] Jie Zhang,[b] Lei Sun,[b] Zhiquan Huang*[c] and Hulin Zhang*[b]

[a]College of Electronic Information Engineering, Taiyuan University of Technology, Taiyuan, 030024, China

[b]College of Integrated Circuits, Taiyuan University of Technology, Taiyuan, 030024, China

[c]School of Mechanical Engineering, Taiyuan University of Science and Technology, Taiyuan, 030024, China

*To whom correspondence should be addressed: zhiquanhuang@tyust.edu.cn (Z.H.); zhanghulin@tyut.edu.cn (H.Z.)

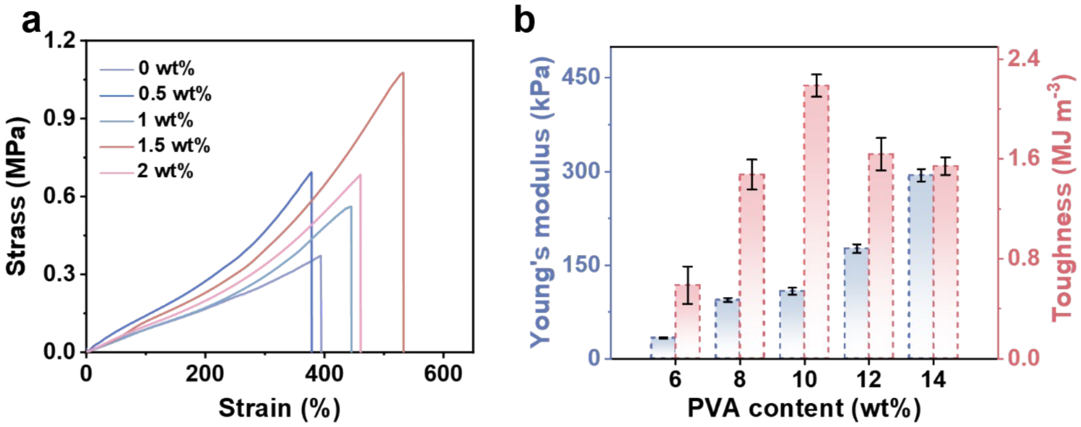

Figure S1. (a) Tensile stress-strain curves with different CG contents. (b) Young's modulus and toughness of the PCPG with different PVA contents.

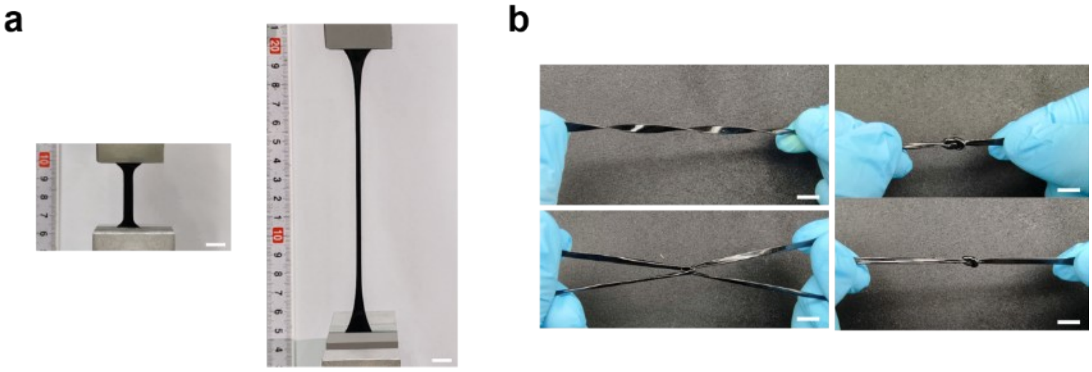

Figure S2. (a) The photo shows the hydrogel before and after stretching. Scale bar 1 cm. (b) Photographs showing the PCPG exhibits the ability to withstand twisting, knotting, and cross stretching. Scale bar 1 cm.

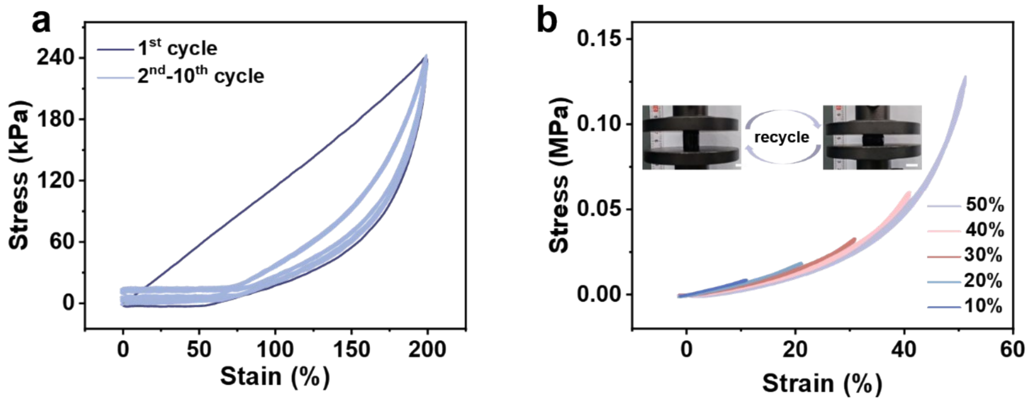

Figure S3. (a) Cyclic stretching-releasing curves with strain of 200%. (b) Cyclic compression-releasing curves. The illustration is a compression-recovery image. Scale bar 1 cm.

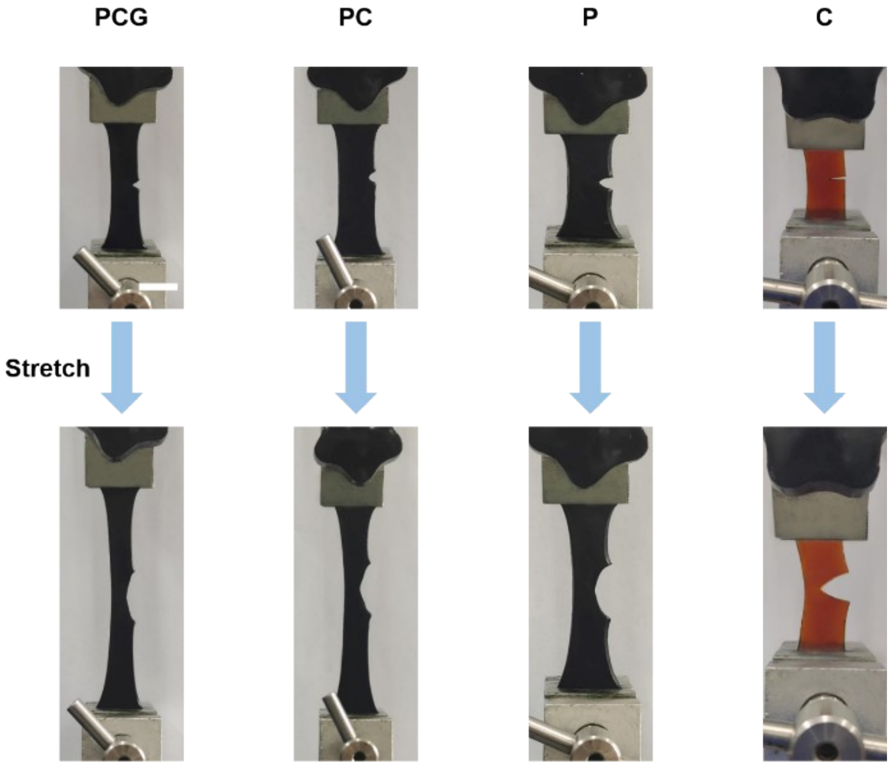

Figure S4. Pre-stretch and post-stretch images of the cracked PCPG with different compositions. Scale bar 2 cm.

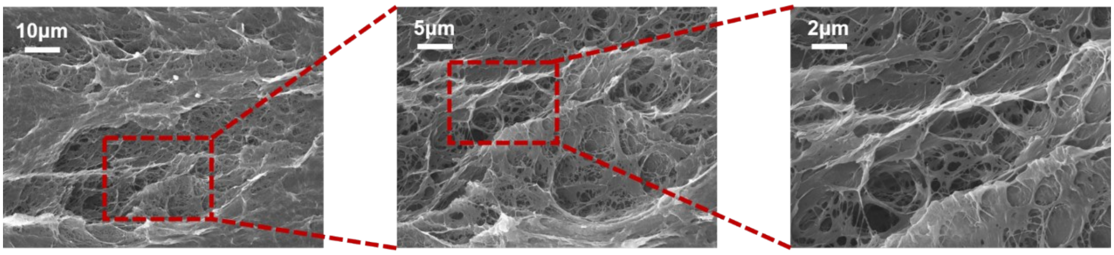

Figure S5. SEM images of the PCPG and corresponding magnified images.

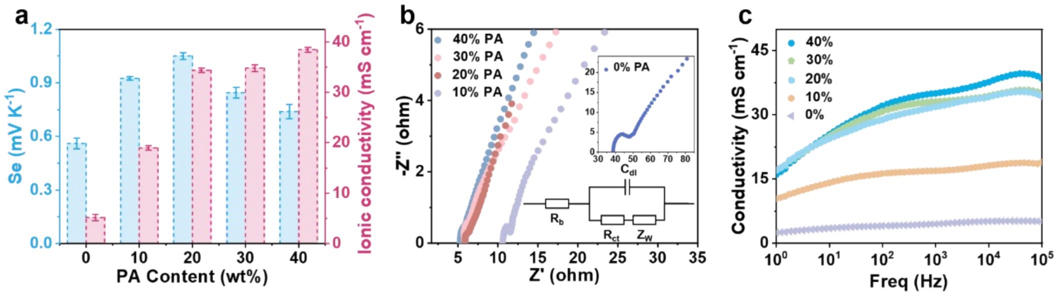

Figure S6. (a) S_e and ionic conductivity of the PCPG with different PA concentrations. (b) The electrochemical impedance spectroscopy (EIS) plots of the PCPG with different PA concentrations and (c) corresponding frequency-dependent ionic conductivity. The illustration shows the internal equivalent circuit of the electrolyte.

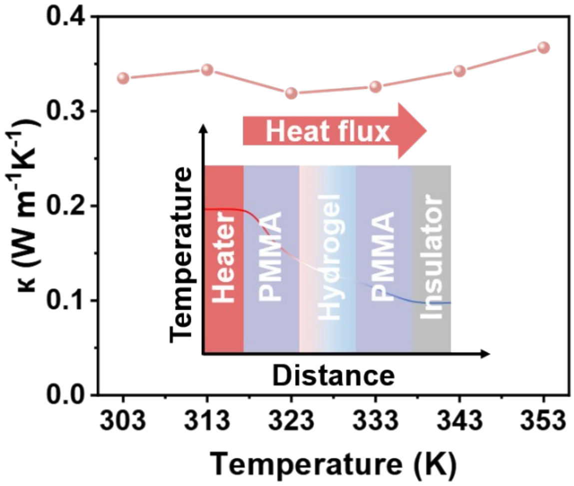

Figure S7. The thermal conductivity of the PCPG under different temperature. The inset is schematic of thermal conductivity measurements using the steady-state method.

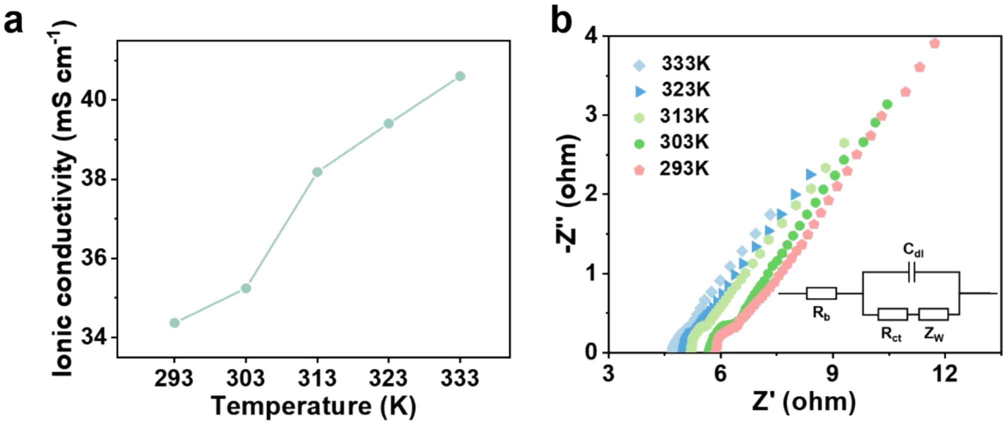

Figure S8. (a) Ionic conductivity of the PCPG under different temperatures and (b) corresponding EIS plots. The illustration shows the internal equivalent circuit of the electrolyte.

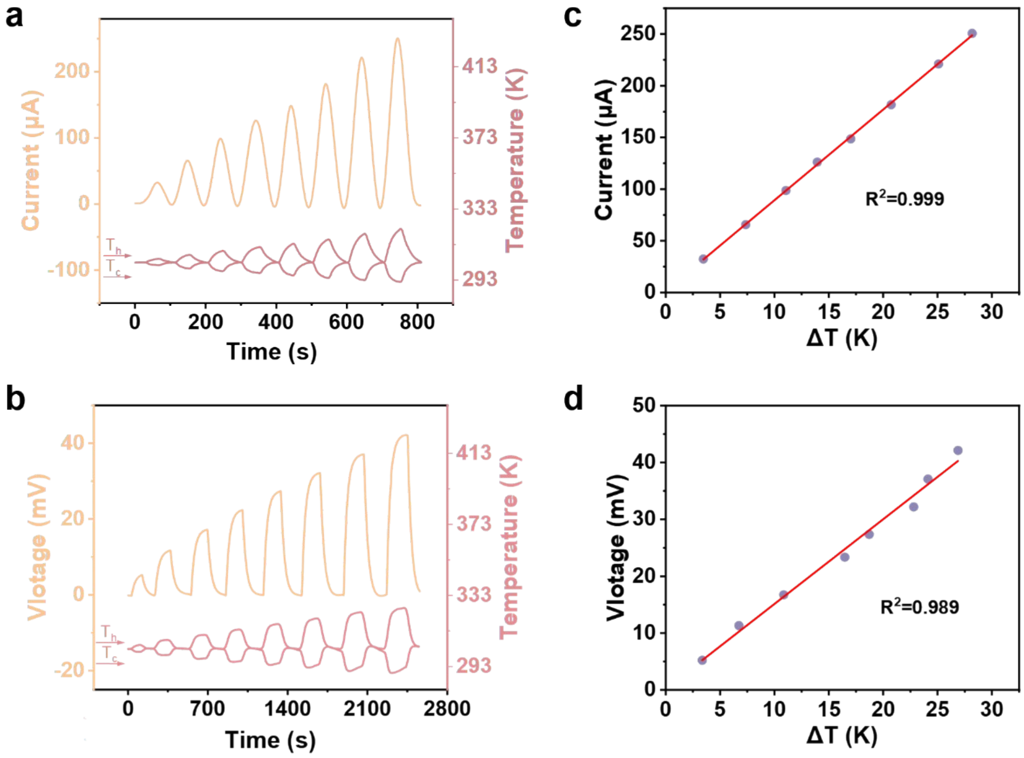

Figure S9. (a) Output voltage and (b) current curves of the thermogalvanic gel at different temperatures. (c,d) The fitted curves are used to illustrate the relationship between voltage/current and temperature difference.

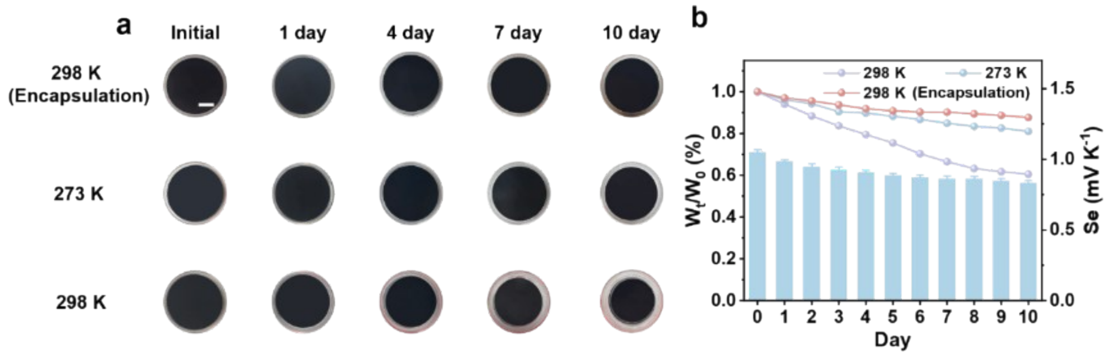

Figure S10. (a) The size changes, (b) mass and S_e variations of the PCPG after being stored under different conditions for 10 days. Scale bar 1 cm.

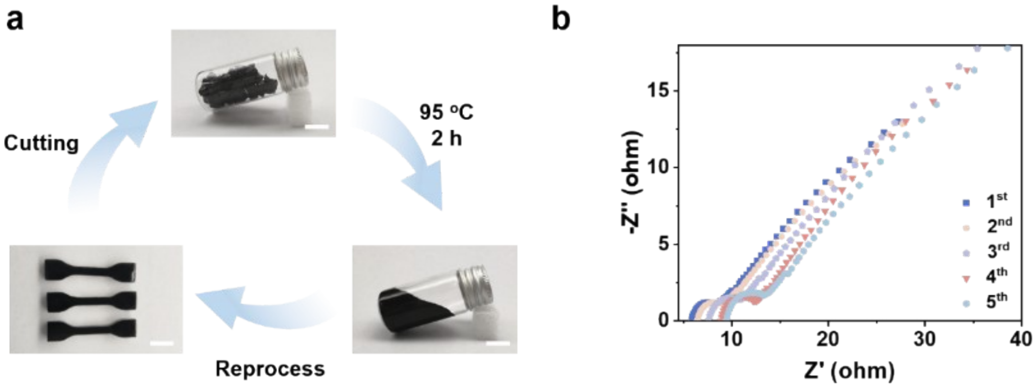

Figure S11. (a) Recycling process of the PCPG. Scale bar 1 cm. (b) EIS plots of the PCPG for 10 days.

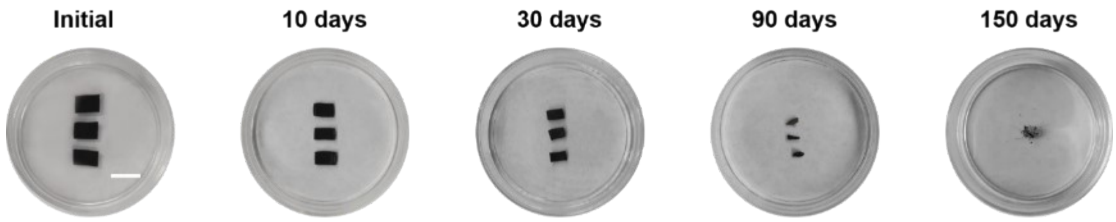

Figure S12. The photos of abandoned PCPG were degraded in soil under natural conditions, which could be degraded in the soil after 150 days. Scale bar 2 cm.

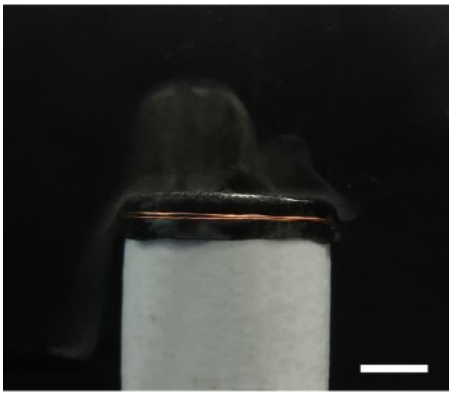

Figure S13. Digital image showing the patch was steamed on top of boiling water. Scale bar 2 cm.

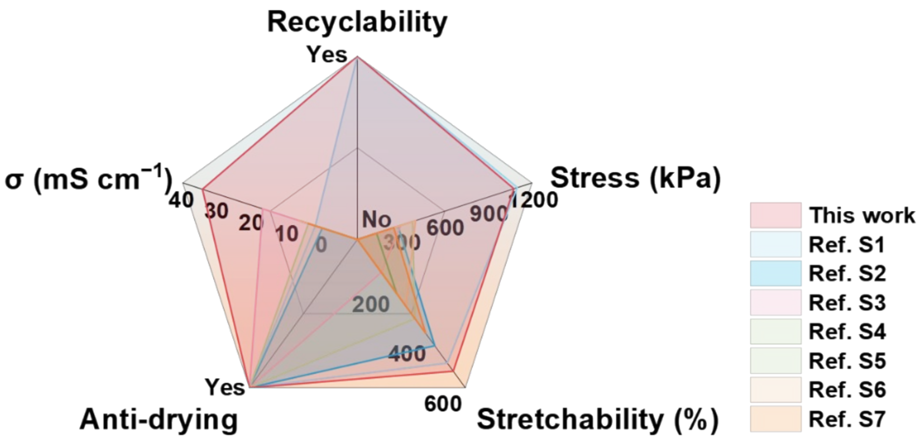

Figure S14. A comprehensive comparison between the PCPG and the previously reported thermogalvanic hydrogels in terms of the comprehensive properties of stretchability, stress, recyclability, ionic conductivity (σ) and anti-drying. The references and details are summarized in Table S1.

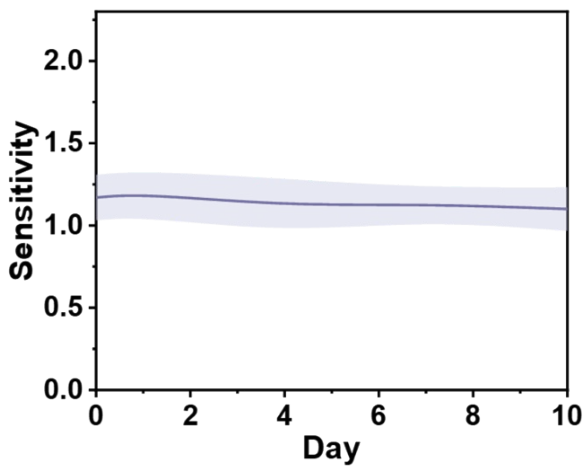

Figure S15. Sensitivity variation of the PCPG over 10 days at room temperature.

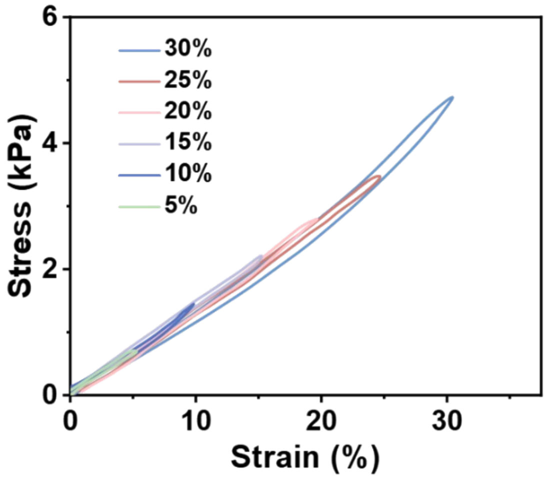

Figure S16. Cyclic tensile loading-unloading curves of the hydrogel under different strains (0-30%).

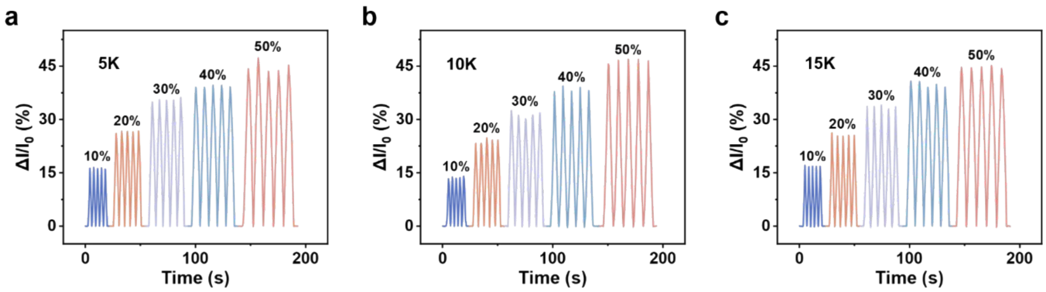

Figure S17. (a-c) Current output after stabilization at 5 K, 10 K, and 15 K temperature differences and current changes at 10%, 20%, 30%, 40%, and 50% tensile strains.

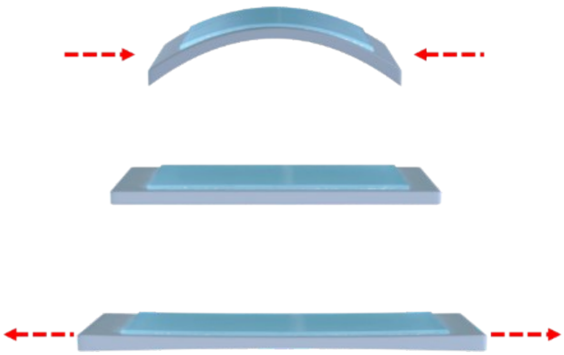

Figure S18. Illustrations of facial muscle deformation for different actions.

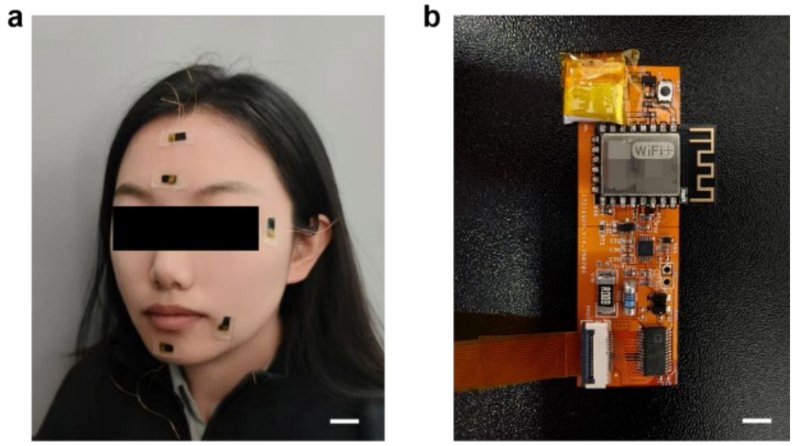

Figure S19. (a) The digital image of the hydrogel array assembly on the face. Scale bar 3 cm. (b) Flexible wireless multichannel sensing module. Scale bar 1 cm.

Figure S20. Relative current changes of the 6 expressions.

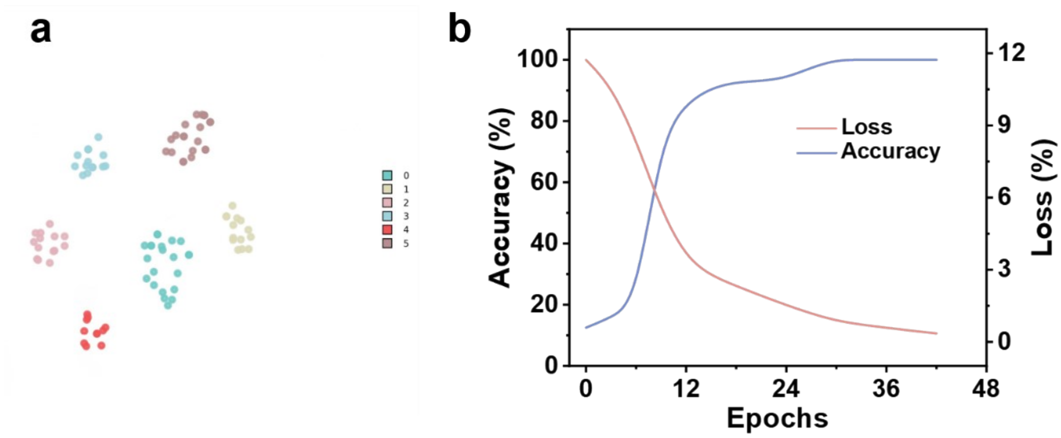

Figure S21. (a) The distribution of datasets in a two-dimensional space. 0 to 5 correspond to happy, disgust, angry, sad, fear, surprise, respectively. (b) Accuracy and loss curves of recognizing 6 expressions.

Table S1. A comparison of the PCPG with other representative reported thermogalvanic hydrogels in terms of stretchability, stress, recyclability, ionic conductivity (σ) and anti-drying.

Stress (%)	Stretchability (kPa)	Recyclability	σ (mS cm^{-1})	Anti-drying	Ref.
533	1075	Yes	34.4	Yes	This work
500	1100	Yes	2.05	Yes	1
430	280	No	0.06	Yes	2
133	298	No	17.1	Yes	3
320	380	No	4	Yes	4
219	132	No	6	No	5
270	400	No	6.9	No	6
380	250	No	4	No	7

Supplemental references:

1. X. R. Zhang, N. Li, X. J. Cui, Y. Li, Z. S. Wang, K. Zhuo and H. L. Zhang, *J. Mater. Chem. C*, 2024, **12**, 12064-12074.

2. X. B. Li, X. Xiao, C. H. Bai, M. Mayer, X. J. Cui, K. Lin, Y. H. Li, H. L. Zhang and J. Chen, *J. Mater. Chem. C*, 2022, **10**, 13789-13796.

3. J. N. Li, Z. S. Wang, S. A. Khan, N. Li, Z. Q. Huang and H. L. Zhang, *Nano Energy*, 2023, **113**, 108612.

4. X. Li, J. Li, T. Wang, S. A. Khan, Z. Yuan, Y. Yin and H. Zhang, *ACS Appl. Mater. Interfaces*, 2022, **14**, 48743–48751.

5. S. T. Kong, Z. F. Huang, Y. Hu, Y. W. Jiang, Y. Y. Lu, W. W. Zhao, Q. W. Shi, M. Yuan, B. Y. Dai, J. H. Li, W. J. Yang and Y. N. Xie, *Nano Energy*, 2023, **115**, 108708.

6. Y. D. Zong, H. B. Li, X. Li, J. Lou, Q. J. Ding, Z. Q. Liu, Y. F. Jiang and W. J. Han, *Chem. Eng. J.*, 2022, **433**, 134550.

7. P. Peng, Z. Li, D. B. Xie, K. H. Zhu, C. Y. Du, L. R. Liang, Z. X. Liu and G. M. Chen, *J. Mater. Chem. A*, 2023, **11**, 6986-6996.